Two examples of known sources are shown in the left panel of Figure 2.12. While ground-based instruments observe at frequencies up to $\log \nu = 11.45$, PICO's data will extend to the peak of the SED, up to $\log \nu = 11.9$ (Fig. 2.12, left).

A straightforward extrapolation of the *Herschel* counts to the 70% non-Galactic sky gives a detection of 4,500 strongly-lensed galaxies with a redshift distribution peaking at $2 \lesssim z \lesssim 3$ [158], but extending up to $z > 5$ (Fig. 2.12, left panel). If objects like the $z = 5.2$ strongly lensed galaxy HLSJ091828.6+514223 exist at higher redshifts, they will be detectable by PICO out to $z > 10$. At the 600 GHz detection limit, about 25% of all detected extragalactic sources will be strongly lensed; for comparison, at optical/near-IR and radio wavelengths, where intensive searches have been carried out for many years, the yield is only about 0.1%, that is more than two orders of magnitude lower [159]. To add to the extraordinary sub-mm lensing bonanza, the selection of PICO-detected strongly lensed galaxies will be extremely easy because of their peculiar sub-mm colors (Fig. 2.12, left panel), resulting in a selection efficiency close to 100% [160]. The survey will give the brightest objects over the entire sky, maximizing the efficiency of selecting sources for follow-up observations.

The intensive high spectral and spatial resolution follow-up campaign of this large sample will enable a leap forward in our understanding of the processes driving early galaxy evolution and open up other exciting prospects, both on the astrophysical and on the cosmological side (see for example Treu [159]).

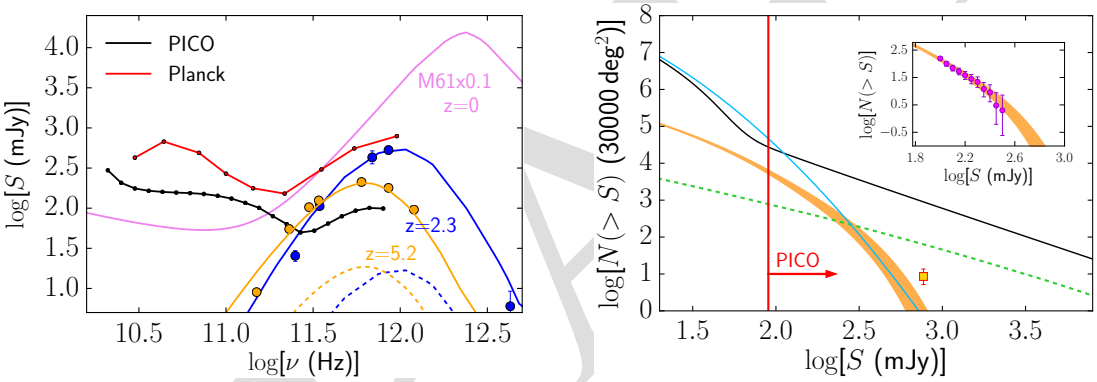

Figure 2.12: **Left:** PICO will detect thousands of new strongly lensed galaxies near the peak of their spectral energy distributions (SEDs), such as SMM J2133-0102 (blue) at $z = 2.3$ [161] and HLSJ091828.6+514223 (orange) at $z = 5.2$ [162]. The dashed lines are the SEDs pre-lensing-induced magnification. PICO's higher resolution gives point-source detection limits (black line) that are up to 10 times fainter compared to *Planck*'s 90% completeness limits (red line [163]). High frequency measurements ($\nu > 300$ GHz) of 30,000 low-z galaxies, like M61 (magenta, SED was scaled down by a factor of ten.), will give a census of their cold dust. **Right panel.** Integral counts of unlensed (black) and strongly lensed, high-z (orange) star-forming galaxies for 70% of the sky away from the Galactic plane at 600 GHz based on fits of *Herschel* counts over 1000 deg^2 (inset [158]). The PICO detection region (right of vertical red line) will yield a factor of 1000 increase in strongly lensed galaxies relative to *Planck* (yellow square), as well as about 50,000 proto-clusters (blue) and 2,000 radio sources (green) [164].

2.5.2 Early Phases of Cluster Evolution

PICO will open a new window for the investigation of early phases of cluster evolution, when their member galaxies were actively star forming (and dusty), but the hot IGM was not necessarily in place. In this phase, traditional approaches to cluster detection (X-ray and SZ surveys, and searches for galaxy red sequences) work only for the more evolved clusters, which do include hot IGM; indeed these methods have yielded only a handful of confirmed proto-clusters at $z \gtrsim 1.5$ [165].[9] *Planck* has demonstrated the power of low-resolution surveys for the study of large-scale structure [166], but its resolution was too poor to detect individual proto-clusters [164]. Studies of the high-z 2-point correlation function [164, 167] and *Herschel* images of the few sub-mm bright protoclusters detected so far, at z of up to 4 [168–170], all of which will

[9] More high-z proto-clusters have been found by targeting the environment of tracers of very massive halos, such as radio-galaxies, QSOs, sub-mm galaxies. These searches are, however, obviously biased.

be detected by PICO, indicate sizes of $\simeq 1'$ for the proto-cluster cores, nicely matching the PICO FWHM at the highest frequencies.

PICO will detect 50,000 proto-clusters as peaks in the high frequency maps, which are not available for ground-based instruments (Table 2.1; blue line in the right-hand panel of Fig. 2.12). The redshift distribution will extend out to $z \sim 4.5$. This catalog will be augmented by 150,000 evolved clusters, detected by the SZ effect. This will constitute a breakthrough in the observational validation of the formation history of the most massive dark-matter halos, traced by clusters, a crucial test of models for structure formation. Follow-up observations will characterize the properties of member galaxies, probing galaxy evolution in dense environments and shedding light on the complex physical processes driving it.

2.5.3 Additional Products of PICO Surveys

PICO will yield a complete census of cold ($15-25$ K) dust, available to sustain star formation in the nearby Universe, by detecting tens of thousands of galaxies mostly at $z \lesssim 0.1$; the SED of M61 is a typical example (Fig. 2.12, left). With a statistical population, and information only available using data at frequencies above 300 GHz, we will investigate the spectral energy distribution of the dust as a function of galaxy properties, such as morphology, and stellar mass.

PICO will increase by an order of magnitude the number of blazars selected at sub-mm wavelengths and will determine the SEDs of many hundreds of them up to 800 GHz and up to $z > 5$. Blazar searches are the most effective way to sample the most massive black holes at high z because of the Doppler boosting of their flux densities. PICO's surveys of the largely unexplored mm/sub-mm spectral region will also offer the possibility to discover new transient sources or events, such as blazar outbursts [171].

PICO will make a leap forward in the determination of the polarization properties of both radio sources and of dusty galaxies over a frequency range where ground-based surveys are impractical or impossible. At 320 (800) GHz it will find 1,200 (500) radio sources and 350 (15,000) dusty galaxies at flux limit down to 4 (6) mJy. These data will give information on the structure and ordering of dusty-galaxies' large-scale magnetic fields. In the case of radio sources emission at higher frequencies comes from regions closer to the central engine, providing information on the innermost regions of the jets, close to the active nucleus.

The anisotropy of the cosmic infrared background (CIB), produced by dusty star-forming galaxies over a wide redshift range $0 < z \lesssim 5$, is an excellent probe of the history of star-formation across time. The *Planck* collaboration derived values for parameters describing the rate of star-formation out to $z \sim 4$ [172–174]). PICO's lower noise and twice the number of frequency bands will give an order of magnitude improvement on the statistical errors for these parameters [175]. Similar improvement will be achieved in constraining $M_{\rm eff}$, the galaxy halo mass that is most efficient in producing star-formation activity. PICO's increased sensitivity to Galactic dust polarization will enhance the separation of signals coming from the largely unpolarized CIB and polarized Galactic dust; an effective separation of signals currently limits making reliable, legacy-quality CIB maps. By providing a nearly full-sky map of matter fluctuations traced by dusty star-forming galaxies, such a set of maps could be used for delensing the CMB [176], for measuring local primordial non-Gaussianity from CIB auto-correlations [177], or for cross-correlations with CMB lensing and with galaxy surveys [107].

2.6 Signal Separation

2.6.1 The Signal Separation Challenge

In the PICO frequency range there are Galactic emissions from free-free, synchrotron, and dust, which arise respectively from free electron-proton scattering, free electrons spiraling around Galactic magnetic field lines, and from ~20 K elongated interstellar dust grains partially aligned with the local magnetic field. The emission from synchrotron and dust are linearly polarized, and data from *Planck* indicates that their level of E-mode is approximately twice that of B [178]. Extra-Galactic sources of emission include the CMB, which has both E and B-modes, and point sources of various types whose polarization level and type are

not well constrained. The task of 'signal separation' is to decompose the detected signal to its constituent sources. The precision of signal separation is determined by the requirement to detect or set an upper limit on the inflationary B-mode, which is the faintest among PICO's targeted signals. In that context, the terms 'foreground separation' and 'foreground cleaning' are used as equivalents to 'signal separation'.

Galactic emission dominates the sky's polarized intensity on large angular scales $\ell \lesssim 10$, it dominates the cosmological B-modes signals for $\ell \lesssim 150$ for all allowed levels of r, and it is expected to be significant even at $\ell \simeq 1000$, posing challenge for reconstructing the B-mode signal from lensing. This is illustrated in Fig. 2.1 and 2.13, which show Galactic emission power spectra calculated based on the cleanest – that is, the least Galactic-emission-contaminated – 60% of the sky. But even in small patches of the sky, far from the Galactic plane and with the least foreground contamination, Galactic emission levels are substantial relative to an inflationary signal of $r \sim 0.01$ and overwhelm it for $r \lesssim 0.001$ [178]. Separating the cosmological and Galactic emission signals (together with control of systematic uncertainties) are *the* challenges facing any next-decade experiment attempting to reach these levels of constraints on r.

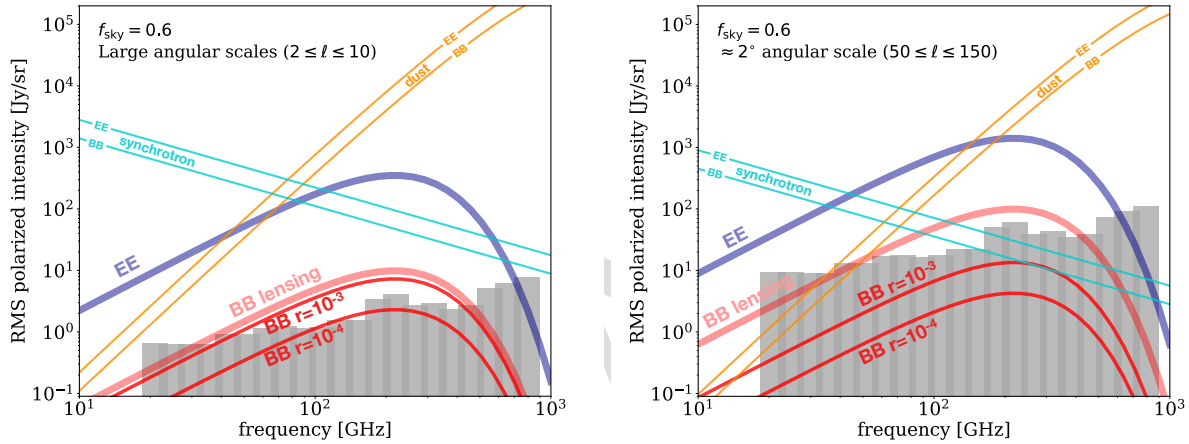

Figure 2.13: Polarization BB spectra of Galactic synchrotron and dust, compared to CMB polarization EE and BB spectra of different origins for two values of r and for two ranges of angular scales: large $\ell \leq 10$, corresponding to the reionization peak (left panel); and intermediate $50 \leq \ell \leq 150$, corresponding to the recombination peak (right panel). The locations and sensitivities of the 21 PICO frequency channels are shown as vertical gray bands.

Foreground separation is challenging because the spatial power spectra and frequency spectra of the foregrounds are not known to sufficient accuracy anywhere across the sky. To a first approximation, the spectrum of synchrotron emission is a power law $I_{\rm sync} \propto \nu^{\alpha}$, with $\alpha \simeq -1$. The spectrum of dust emission is $I_{\rm dust} \propto \nu^{\beta} B_{\nu}(T_{\rm dust})$, where $\beta \simeq 1.6$, $T_{\rm dust} \simeq 20\,{\rm K}$, and $B_{\nu}(T)$ is the Planck function; this is referred to as 'modified blackbody emission'. If those models exactly reflected the properties of emitting sources, then in principle an experiment that had six frequency bands could determine the three emission parameters, as well as the three amplitudes corresponding to that of dust, synchrotron, and the CMB. However, recent observations have shown that neither emission law is universal, that spectral parameters are not necessarily the same for intensity and polarization and that they vary across the sky [179–181], and thus that the analytic forms and parameter values given above are valid only as averages across the sky. Also, while both emission laws are well-motivated phenomenological descriptions, the fundamental physics of emissions from grains of different materials, sizes, and temperatures, and of electrons spiraling around magnetic fields implies that these laws are expected to be neither exact, nor universal.

At the low levels of r targeted by PICO and by other next-decade experiments, even small inaccuracies in foreground modeling and characterization lead to biases and false detections. For example, several publications have demonstrated that fitting complicated dust temperature profiles using a simple one- or two-temperature model will bias the fitted CMB signal at levels $\delta r \lesssim 10^{-3}$, which is significant compared

to PICO's goal [182–186].

Further complicating the foreground-separation challenge is the fact that additional polarized foregrounds may exist. 'Anomalous microwave emission' (AME), dust-correlated emission peaking in intensity near 30 GHz, is an important low-frequency foreground in total intensity. It has been tentatively identified with small, rapidly-spinning dust grains [131]. Very few measurements of AME polarization exist, and there are only loose constraints on its fractional polarization; it is less than 3% (2σ) at 18 GHz in one 0.5% region of the sky [187]. If AME is 1% polarized, left uncorrected it would give rise to a bias of $\delta r \simeq 5 \times 10^{-4}$ [195]. Astrophysical emission from CO lines at mm wavelengths is expected to be 0.1 - 1% polarized [188, 189]. Extragalactic radio sources show a median polarization of 2% [190–192], and next to no information is available about the polarization of dusty-galaxies emitting in the PICO wave-bands. Initial quantitative estimates show that ignoring CO lines and radio sources may each lead to a bias $\delta r \simeq 1 \times 10^{-3}$ [193, 194]. These levels are appreciable compared to PICO's and other next-decade experiments' goals.

2.6.2 Foreground Separation Assessment and Methodology

Two broad approaches are used for foreground separation and for assessment of its precision. In the parametric approach the foregrounds are assumed to follow emission laws described by a number of free parameters. Parametric models use the frequency dependence of the data in each line of sight to determine the values of the parameters [196]. Since the CMB spectrum is well determined, measurements with a sufficient number of frequency bands and appropriately broad frequency coverage can distinguish foreground emission from the CMB using their different spectral dependences. Non-parametric techniques, in contrast, rely on the fact that CMB emission is uncorrelated with the foregrounds and thus correlations within a given spatial/frequency data-cube can be used to separate the two distinct sources of emission [197, 198]. Simulated data are used to assess the efficacy of both techniques as a function of increasing complexity for the assumed foreground emission. For the parametric models, we can also employ analytic methods to estimate the uncertainty on emission parameters as a function of instrument noise, but specific assumptions must be made about the underlying nature of the emission laws [199].

To investigate the efficacy of PICO to address the foreground-separation challenge, we used both an analytic forecast and map-domain simulations.

• **Analytic Forecast** The analytic forecast relies on an established, documented, publicly available, cosmological parameters forecasting code [199]. The code uses *Planck*-reported Galactic emissions; it assumes that the foreground spectral indices are constant across patch sizes of ∼15 deg on a side; it employs a parametric maximum-likelihood approach to remove the foregrounds and to forecast $\sigma(r)$; and it uses the cleanest 60% of the sky. Lensing B-modes are included in the input spectra (and are partially removed via delensing, taking into account noise and residual foregrounds), but the input for the inflationary signal is $r = 0$. Results from the publicly available code, have been verified using a second, entirely independent code that uses similar analytic calculations.

• **Map-Domain Simulations** Map-domain simulations have become the 'gold standard' in the community. In this approach, we simulate sky maps that are constrained by available data, but otherwise have a mixture of foreground properties. We 'observe' these maps just like a realistic experiment would do, and then apply foreground separation techniques – both parametric and non-parametric – to separate the Galactic and CMB emissions.

We constructed eight different full-sky models. All models are consistent with available data and with uncertainties from WMAP and *Planck*. The range of models include varying degrees of complexity, including spectral parameters varying spatially and along the line of sight, anomalous microwave emission up to 2% polarized, dust polarization that rotates slightly as a function of frequency because of projection effects, or dust SEDs that depart from a simple modified blackbody. All foreground maps were generated at native resolution of 6.8 arcmin pixels [201] with widely-used and thoroughly-tested map-generation codes [119, 200]. Fig. 2.14 shows two of the eight models and data from *Planck*. The right panel is constructed to mimic the

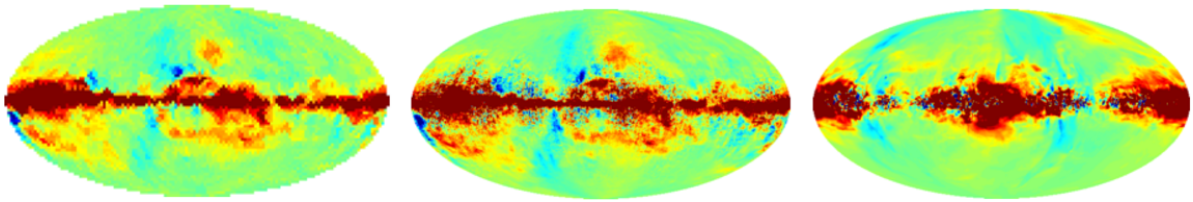

Figure 2.14: Foreground maps: *Planck* real sky (left) at 143 GHz, models at 155 GHz from PySM (middle) [200] and Galactic MHD simulations (right). The model generated by MHD simulations is only constrained to match *Planck* Galactic foregrounds spatial power spectra, not the actual spatial realization.

Planck Galactic emissions statistically. The middle panel is constructed to mimic the observed spatial distribution of Galactic emission. The difference with the *Planck* map illustrates that different realizations of the sky are allowed by current data, and highlights the level of current Galactic emission uncertainties.

For each of the eight models, we added CMB signals in both intensity and polarization, matching a ΛCDM universe. The input inflationary signal was $r = 0$, namely, no signal, and the *BB*-lensing matched the level after 85% delensing as forecasted for PICO. Each of these sky models had 50 realizations of the PICO noise level. The sky models were analyzed with a variety of techniques, which were based on the two broad categories described above. Because of limited resources not all models were analyzed with all techniques, and not all realizations were used.

2.6.3 Results and Discussion

When using the PICO baseline noise levels with the analytic forecasts we find that $\sigma(r) = 2 \times 10^{-5}$, a level that is five times lower than required ($\sigma(r) = 1 \times 10^{-4}$, see SO1). We consider this forecast optimistic because it assumes strictly white noise, a specific model for the underlying foregrounds that has only eight parameters[10] per 15×15 deg^2 pixel, and Gaussian parameter likelihood functions. The foregrounds may be more complex, requiring more parameters (for example, spatially varying temperature for the dust, or more than a single spectral index per source of emission), and may have stronger spatial variations. The parameter likelihoods may not be Gaussian.

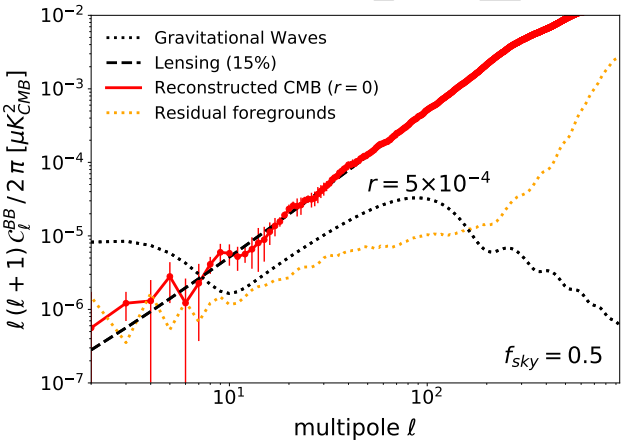

Figure 2.15: Angular power spectra of *BB* due to the CMB and of residual foregrounds after an end-to-end map-based foreground-separation exercise. The PICO low noise levels and breadth in frequency coverage enable suppression of foregrounds such that the residual foreground spectrum (yellow dots) is a factor of ten (four) below a *BB* inflationary signal with $r = 5 \times 10^{-4}$ (black dots). Within errors, the recovered CMB (red) matches the input CMB, which consists of only lensing *BB* (dash black), over all angular scales $\ell \gtrsim 6$. In this exercise we used 50% of the sky. Lower foreground residual levels are obtainable with smaller, cleaner patches of ∼10% of sky, which would reduce the residual foregrounds at $\ell \simeq 80$.

The 'gold-standard' map-based simulations give initial evidence that the combination of PICO's sensitivity and broad frequency coverage are effective in foreground removal and that PICO will reach the requirement of $r = 5 \times 10^{-4} (5\sigma)$. Fig. 2.15 shows the result of a foreground-separation exercise over 50% of the sky, with one representative model of Galactic emissions, and using GNILC, one of the non-parametric techniques [198]. In this exercise GNILC was tuned to give low foregrounds on the largest angular scales, that is, the lowest ℓ modes. The input CMB *BB* signal, consisting of only lensing *B*-modes, is reconstructed

[10] Six amplitudes for the Q and U Stokes parameters of the CMB, dust, and synchrotron emission, and two spectral indices, for dust and synchrotron.

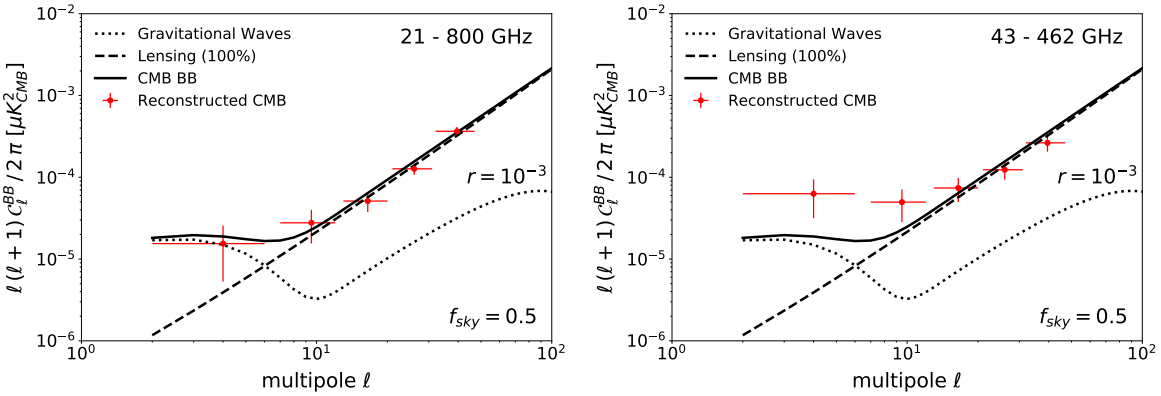

Figure 2.16: Foreground separation with all of PICO's 21 frequency bands recovers the input CMB *BB* power spectrum (solid black, left and right) without bias (left, red). The input CMB spectrum has contribution from lensing (dash, left and right) and an inflationary signal with $r = 0.001$ (dots, left and right). This exercise uses a parametric approach [*196*] with foregrounds varying on 4° pixels, and using 50% sky fraction. Running the same algorithm on the same sky but using only PICOs bands between 43 and 462 GHz produces an output spectrum (right, red) that is biased at low multipoles relative to the input. With real data, the bias would be erroneously interpreted as higher value of r.

within errors for all $\ell \gtrsim 6$. The residual foreground *BB* power spectrum, encoding the levels of remaining foreground emission after foreground-separation, is a factor of 50 (5) below the CMB at $\ell = 100\,(10)$. Most importantly, the residual foreground is a factor of ten below an inflationary *BB* signal for $r = 5 \times 10^{-4}$ at $\ell \simeq 4$. These are the angular scales at which the inflationary signal is stronger than the signal from lensing. Comparing the residual foreground at this ℓ to the input *BB* foregrounds at, for example, 155 GHz (Fig. 2.1) we find a suppression of $\sim 10^6$ in μK^2 (a factor of 1000 in temperature), which is a consequence of using *all* of PICO bands.

At intermediate angular scales $\ell \simeq 80$ the residual foreground is a factor of four lower than the inflationary signal. We expect lower residuals when GNILC is optimized for this ℓ range. And for reconstructing signals at this ℓ range, it is sufficient to analyze data from smaller ∼3% regions of the sky. These will have lower mean foregrounds levels, making the foregrounds-separation exercise easier, and pushing residuals to levels lower than already demonstrated here for 50% of the sky. With its full sky coverage, PICO will have access to several independent 3% sky patches, and will thus make several independent detections of its r target.

Our results validate the need for a broad frequency coverage with a strong lever arm on Galactic emissions outside of the primary CMB bands. Fig. 2.16 shows that removing several of PICO's frequency bands, particularly those that monitor dust and synchrotron at high and low frequencies, respectively, significantly biases the extracted *BB* power spectrum, especially at the lowest multipoles. In this exercise the input CMB contained the lensing signal *and* an inflationary signal with $r = 0.001$.

While these results suggest that PICO's frequency coverage and sensitivity will be adequate for this level of r, more work should be invested to gain complete confidence. For example, some of the other sky models give level of residual foregrounds that would give biased measurements reflecting much larger values of r, even with PICO's low noise and broad frequency coverage; and some of the foreground-separation techniques appear to give consistently higher foreground residuals than others. To make progress, it is important (1) to measure Galactic emissions with ground- and balloon-based experiments and thus constrain the level of uncertainties, and (2) to continue the simulations and algorithm development program consisting of running numerous realizations of different sky models, and analyzing them with various approaches; optimizing sky masks; and using combination of techniques to handle large, intermediate, and small angular scale foregrounds differently.